Damping in Beams with Multiple Dry Friction Supports

D. M. Tang,* E. H. Dowell,† and J. E. Albright‡
Duke University, Durham, North Carolina

An equivalent linear viscous damping formula for beams with rather general dry friction support conditions is proposed. The effect of normal force support reaction at the dry friction support on response is also discussed. Comparisons of experimental results to those obtained from an approximate solution and numerical time integration are made. Generally good agreement is found among the several results.

Nomenclature

a	= beam length, cm
a_{d1}, a_{d2}	= positions of dry friction support, cm
$\bar{a}_{d1}$, $\bar{a}_{d2}$	= $a_{d1} = a_{d1}/a$, $a_{d2} = a_{d2}/a$
a_n	= modal generalized coordinate, cm
b	= beam width, cm
E	= modulus of elasticity, kg/cm^2
$F(t)$, F_0, or F	= force and force amplitude, kg
f	= excitation frequency, Hz
f_n, ω_n	= nth mode natural frequencies of beam, Hz, rad/s
h	= beam thickness, cm
I	= beam moment of inertia, cm^4
K, k	= total number of dry friction supports, support number
M_n	= generalized mass of nth mode, kg·s^2/cm
m	= mass per unit length, kg·s^2/cm^2
N_{g1}, N_{g2}	= normal load, kg
N_{xi}	= horizontal resultant for ith span beam, kg
n	= mode numbers
T, t	= time, s
u, w, or W	= horizontal and lateral beam displacement, cm
w_r	= lateral beam displacement with support reaction included, cm
X	= x/a
x	= Cartesian position coordinate on beam
x_F	= force position, cm
δ	= $1 - w_r/w$
ϕ_n	= modal function of nth mode
μ	= coefficient of friction
ζ_n	= equivalent damping ratio of nth mode
$()'$	= derivative with respect to x
$(\dot{})$	= time derivative

Introduction

DRY friction is often encountered in engineering structures. Because of its ability to dissipate energy, dry friction damping has been purposely applied to mechanical systems to reduce their vibration levels and improve control performance. However, introducing dry friction makes the analytical model more complex and the prediction of system behavior more difficult. Much of the previous work[1-12] was done to develop some analytical technique for application to a dry friction damped system. The equivalent viscous damping method proposed by Den Hartog[3] and Timoshenko et al.[4] has been the most widely used. Other time and frequency domain methods for a multiple-degree-of-freedom dry friction damped system also have been applied. Comparison of analytical predictions with experimental results has been made as well. An important distinction is between dry friction elements that provide a force in the direction of the principal motion (as in the work of Den Hartog) vs those that provide a force perpendicular to the direction of principal motion as studied in Refs. 1 and 2 and the present paper.

References 1 and 2 proposed an equivalent linear viscous damping formula for beams and plates due to slipping at the support boundaries. The objective of this study is to extend Dowell's formula to beams with more general dry friction support conditions and to provide the basis for an approach to control vibration levels in beams and plates using dry friction damping.

In this paper, an equivalent linear viscous damping is derived based upon the use of component mode synthesis.[12,13] This method has been extended recently to study nonlinear, nonconservative systems. The effect of normal force support reaction at a dry friction support on vibration response (modal damping ratio) is also analyzed. The design of the beam experimental apparatus and the utilization of the associated instrumentation are also described in this paper. Comparisons of the experimental results to those obtained from the approximate solution and numerical time integration are made to confirm the accuracy of the analytical approach. In general, the experimental results are reasonably close to those of the theoretical solutions.

Problem Formulation

Reference 1 gives an expression for equivalent viscous damping due to dry friction in the case of arbitrary lateral boundary conditions at each end of the beam. As an extension, we will discuss damping with multiple dry friction support elements. For example, consider a mathematical model for a pinned-pinned beam with two intermediate dry friction supports. See Fig. 1. The beam is assumed to be uniform. At the dry friction supports $d1$ and $d2$, the normal loads and dry friction coefficients are N_{g1}, N_{g2}, and μ_1, μ_2, respectively. External force F is concentrated at point x_F. The horizontal resultant force in each span beam is N_{x1}, N_{x2}, and N_{x3}.

The natural frequencies and modes of the above given system can be determined using the method presented by Dowell.[13]

Received Dec. 4, 1986; revision received April 20, 1987.

*Visiting Scholar, Department of Mechanical Engineering and Materials Science (on leave from Nanjing Aeronautical Institute, China).
†Dean, School of Engineering.
‡Research Assistant, Department of Mechanical Engineering and Materials Science.

Here, we shall consider two kinds of longitudinal boundary supports: $u(x=0)=u(x=a)=0$ and $u(x=0)=0$, $u(x=a)\neq 0$. Arbitrary lateral end support boundary conditions are allowed.

$u(x=0)=u(x=a)=0$

We simplify our discussion to a single mode. The beam deflection w is expressed in modal form as

$$w(x,t)=a_n(t)\phi_n(x) \tag{1}$$

where $\phi_n(x)$ is the modal function of the given beam.

The total kinetic energy is expressed as

$$T=\tfrac{1}{2}\int_0^a m\dot{w}^2\mathrm{d}x=\tfrac{1}{2}M_n\dot{a}_n^2 \tag{2}$$

where

$$M_n=\int_0^a m\phi_n^2\,\mathrm{d}x$$

The potential energy is defined as

$$V_1=\frac{1}{2}\int_0^a EI\left(\frac{\partial^2 w}{\partial x^2}\right)^2\mathrm{d}x=\frac{1}{2}M_n\omega_n^2 a_n^2$$

$$V_2=\frac{1}{2}\int_0^{a_{d1}} N_{x1}\left(\frac{\partial w}{\partial x}\right)^2\mathrm{d}x+\frac{1}{2}\int_{a_{d1}}^{a_{d2}} N_{x2}\left(\frac{\partial w}{\partial x}\right)^2\mathrm{d}x+\frac{1}{2}\int_{a_{d2}}^{a} N_{x3}\left(\frac{\partial w}{\partial x}\right)^2\mathrm{d}x$$

The total potential energy is

$$V=V_1+V_2 \tag{3}$$

The virtual work can be expressed as

$$\delta W=F\delta w=F\phi_n(x_F)\delta a_n \tag{4}$$

The Lagrangian $L=T-V$ can be formed and Lagrange's equations are

$$\frac{d}{dt}\left(\frac{\partial L}{\partial \dot{a}_n}\right)-\frac{\partial L}{\partial a_n}=Q_n \tag{5}$$

where $Q_n=F\phi_n(x_F)$.

This gives

$$M_n(\ddot{a}_n+\omega_n^2 a_n)+a_n\left[N_{x1}\int_0^{a_{d1}}(\phi_n')^2\,\mathrm{d}x+N_{x2}\int_{a_{d1}}^{a_{d2}}(\phi_n')^2\,\mathrm{d}x+N_{x3}\int_{a_{d2}}^{a}(\phi_n')^2\,\mathrm{d}x\right]=F\phi_n(x_F) \tag{6}$$

For the unknown horizontal resultants N_{x1}, N_{x2}, and N_{x3}, we find the following three additional equations:

If $|N_{x1}-N_{x2}|>\mu_1 N_{g1}$ and $|N_{x2}-N_{x3}|>\mu_2 N_{g2}$, slip occurs at both intermediate supports.

Taking a free-body diagram of the dry friction support $d1$, gives (see Ref. 1)

$$N_{x1}=N_{x2}+\mu_1 N_{g1}\,\mathrm{Sign}\left[a_n\dot{a}_n\int_0^{a_{d1}}(\phi_n')^2\,\mathrm{d}x\right] \tag{7}$$

where the [. . .] term is the in-plane beam velocity at the dry friction support.

In a similar manner, another equation can be obtained from support $d2$,

$$N_{x2}=N_{x3}+\mu_2 N_{g2}\,\mathrm{Sign}\left[a_n\dot{a}_n\int_{a_{d2}}^{a}(\phi_n')^2\,\mathrm{d}x\right] \tag{8}$$

Now we consider the whole beam. It is found that

$$N_{x1}a_{d1}+N_{x2}(a_{d2}-a_{d1})+N_{x3}(a-a_{d2})=\frac{Ehb}{2}a_n^2\int_0^a(\phi_n')^2\,\mathrm{d}x \tag{9}$$

From Eqs. (7–9), one may obtain three equations for N_{x1}, N_{x2}, and N_{x3}. Substituting these into Eq. (6), one may obtain a final nonlinear equation for a_n,

$$M_n(\ddot{a}_n+\omega_n^2 a_n)+a_n^3\frac{Ehb}{2a}\left[\int_0^a(\phi_n')^2\,\mathrm{d}x\right]^2+\frac{a_n}{2a}\times\left\{[t_1(a-a_{d1})+t_2(a-a_{d2})]\int_0^{a_{d1}}(\phi_n')^2\,\mathrm{d}x+[t_2(a-a_{d2})-t_1 a_{d1}]\int_{a_{d1}}^{a_{d2}}(\phi_n')^2\,\mathrm{d}x-[t_1 a_{d1}+t_2 a_{d2}]\int_{a_{d2}}^{a}(\phi_n')^2\,\mathrm{d}x\right\}=F\phi_n(x_F) \tag{10}$$

where

$$t_1=\mu_1 N_{g1}\,\mathrm{Sign}(a_n\dot{a}_n)$$

$$t_2=\mu_2 N_{g2}\,\mathrm{Sign}(a_n\dot{a}_n)$$

If $|N_{x1}-N_{x2}|<\mu_1 N_{g1}$ and $|N_{x2}-N_{x3}|<\mu_2 N_{g2}$, no slip occurs at either intermediate support.

The governing equation is now of the Duffing type, as

$$M_n(\ddot{a}_n+\omega_n^2 a_n)+a_n^3\frac{Ehb}{2}\left\{\frac{1}{a_{d1}}\left[\int_0^{a_{d1}}(\phi_n')^2\,\mathrm{d}x\right]^2+\frac{1}{a_{d2}-a_{d1}}\times\left[\int_{a_{d1}}^{a_{d2}}(\phi_n')^2\,\mathrm{d}x\right]^2+\frac{1}{a-a_{d2}}\left[\int_{a_{d2}}^{a}(\phi_n')^2\,\mathrm{d}x\right]^2\right\}=F\phi_n(x_F) \tag{11}$$

Of course, slipping might only occur at one intermediate support, but not the other.

If $|N_{x1}-N_{x2}|>\mu_1 N_{g1}$ and $|N_{x2}-N_{x3}|<\mu_2 N_{g2}$, the motion equation is

$$M_n(\ddot{a}_n+\omega_n^2 a_n)+a_n^3\frac{Ehb}{2}\left\{\frac{1}{a_{d2}}\left[\int_0^{a_{d2}}(\phi_n')^2\,\mathrm{d}x\right]^2+\frac{1}{a-a_{d2}}\times\left[\int_{a_{d2}}^{a}(\phi_n')^2\,\mathrm{d}x\right]^2\right\}+a_n t_1\left[\int_0^{a_{d1}}(\phi_n')^2\,\mathrm{d}x-\frac{a_{d1}}{a_{d2}}\int_0^{a_{d2}}(\phi_n')^2\,\mathrm{d}x\right]=F\phi_n(x_F) \tag{12}$$

Consider further Eq. (10); we shall simplify our discussion by having the same slipping condition at both supports, i.e.

$$N_{g1}=N_{g2}=N_g \text{ and } \mu_1=\mu_2=\mu$$

The motion equation can be represented as

$$M_n(\ddot{a}_n+\omega_n^2 a_n)+a_n^3\frac{Ehb}{2a}\left[\int_0^a(\phi_n')^2\,\mathrm{d}x\right]^2+a_n D\,\mathrm{Sign}(a_n\dot{a}_n)=F\phi_n(x_F) \tag{13}$$

where

$$D=\frac{\mu Ng}{2a}\left[(2a-a_{d1}-a_{d2})\int_0^{a_{d1}}(\phi_n')^2\,\mathrm{d}x+(a-a_{d2}-a_{d1})\times\int_{a_{d1}}^{a_{d2}}(\phi_n')^2\,\mathrm{d}x-(a_{d1}+a_{d2})\int_{a_{d2}}^{a}(\phi_n')^2\,\mathrm{d}x\right]$$

Now assume simple harmonic motion,

$$F = F_c \cos\omega t + F_s \sin\omega t$$

$$a_n = \bar{a}_n \cos\omega t$$

$$\text{sign}(a_n\dot{a}_n) = -\frac{4}{\pi}\sin 2\omega t$$

$$a_n^3 = \bar{a}_n^3(3\cos\omega t/4 + \cos 3\omega t/4)$$

Using these results in Eq. (13) and balancing harmonics, one obtains

$$M_n(\omega_n^2 - \omega^2)\bar{a}_n + \frac{3}{8}\frac{Ehb}{a}\bar{a}_n^3\left[\int_0^a (\phi_n')^2\,dx\right]^2 = F_c\phi_n(x_F)$$
$$\frac{4}{\pi}D\bar{a}_n = F_s\phi_n(x_F) \tag{14}$$

From Eqs. (14), one can construct a cubic in $\bar{a}_n^2$ that can be used to determine the response.

If the nonlinear stiffness cubic term is neglected in Eqs. (14), then an approximation for the modal damping ratio can be determined as

$$\zeta_n = D/\pi M_n\omega_n^2 \tag{15}$$

$u(x=0)=0$, $u(x=a)\neq 0$

For this case, the horizontal motion of one end boundary pinned support is not constrained. The horizontal resultant N_{x3} is zero.

In this case, the governing equations are

$$M_n(\ddot{a}_n + \omega_n^2 a_n) + a_n\left[N_{x1}\int_0^{a_{d1}} (\phi_n')^2\,dx + N_{x2}\int_{a_{d1}}^{a_{d2}} (\phi_n')^2\,dx\right] = F\phi_n(x_F) \tag{16}$$

where

$N_{x1} = N_{x2} + t_1$ and $N_{x2} = t_2$.

When slip of both supports $d1$ and $d2$ occurs, one may obtain a nonlinear equation for a_n,

$$M_n(\ddot{a}_n + \omega_n^2 a_n) + a_n D_{12}\,\text{Sign}(a_n\dot{a}_n) = F\phi_n(x_F) \tag{17}$$

where

$$D_{12} = (\mu_1 N_{g1} + \mu_2 N_{g2})\int_0^{a_{d1}} (\phi_n')^2\,dx + \mu_2 N_{g2}\int_{a_{d1}}^{a_{d2}} (\phi_n')^2\,dx$$

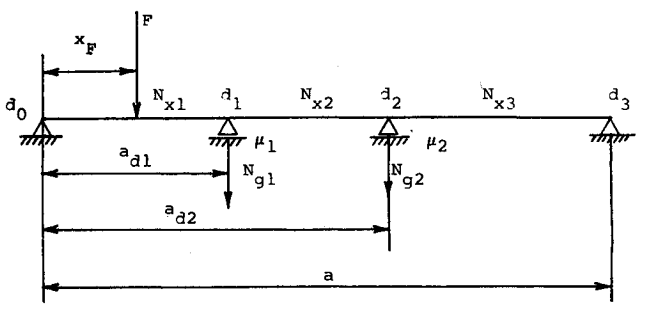

Fig. 1 Beam geometry.

When slip of only one support d_2 occurs, the motion equation is

$$M_n(\ddot{a}_n + \omega_n^2 a_n) + \frac{Ehb}{2a_{d1}}a_n^3\left[\int_0^{a_{d1}} (\phi_n')^2\,dx\right]^2 + a_n D_2\,\text{Sign}(a_n\dot{a}_n) = F\phi_n(x_F) \tag{18}$$

where

$$D_2 = \mu_2 N_{g2}\int_{a_{d1}}^{a_{d2}} (\phi_n')^2\,dx$$

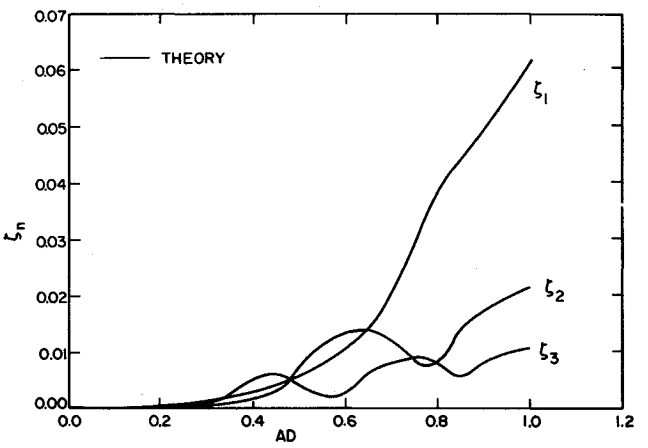

a) Modal damping vs $\bar{a}_d$.

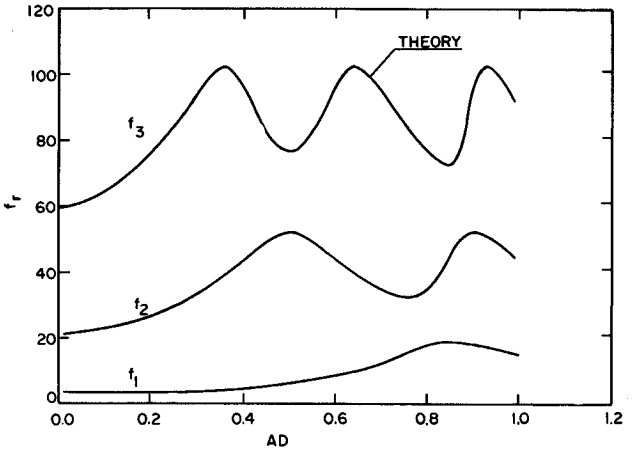

b) Natural frequencies vs $\bar{a}_d$.

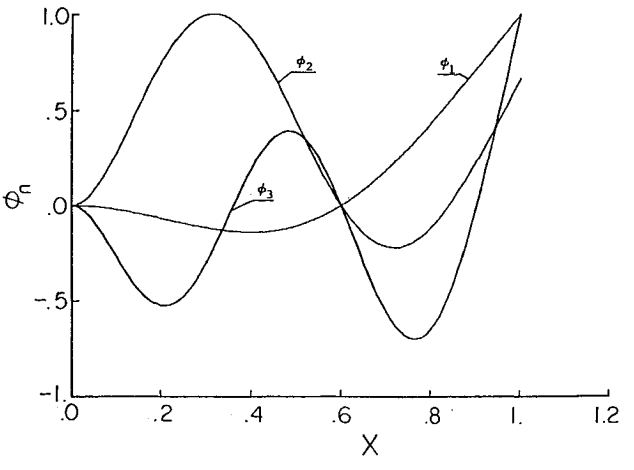

c) Mode shapes, $\bar{a}_d = 0.6$.

Fig. 2 Cantilevered beam with a pinned dry friction support.

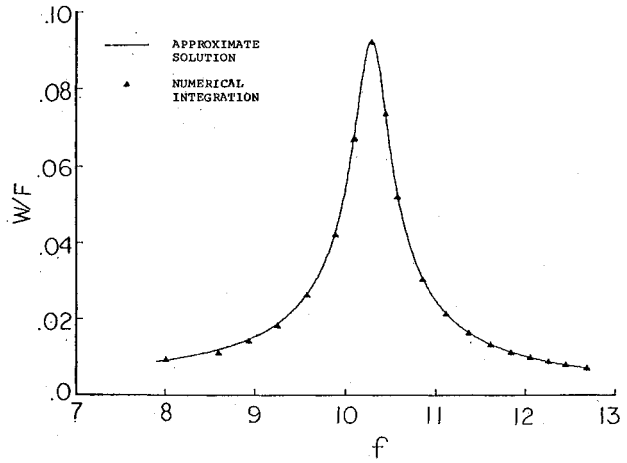

a) Frequency response curve, $F_0 = 1$ kg.

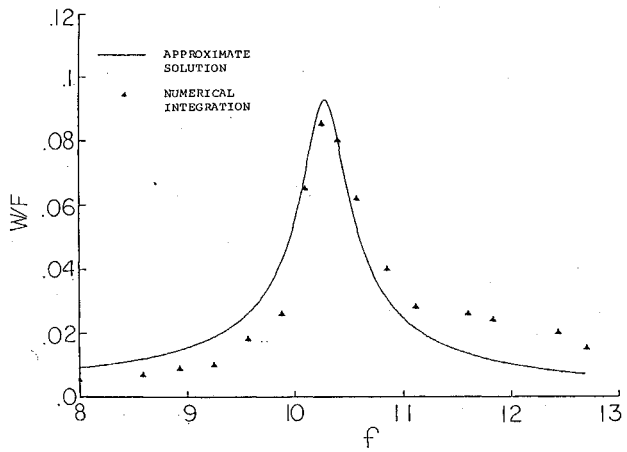

b) Frequency response curve, $F_0 = 0.1$ kg.

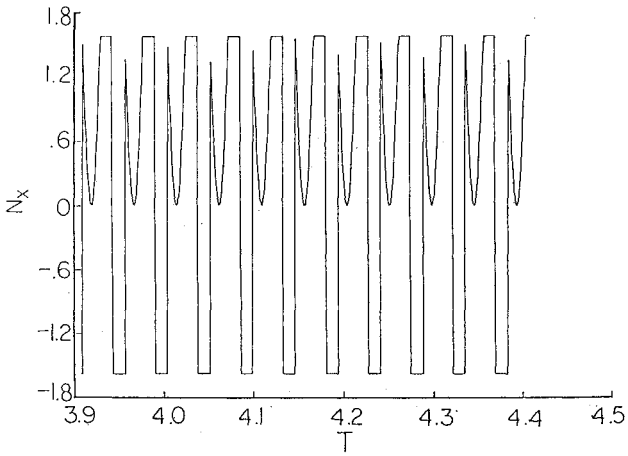

c) Time history of dry friction force, $F_0 = 0.1$ kg, $f = 10.573$ Hz.

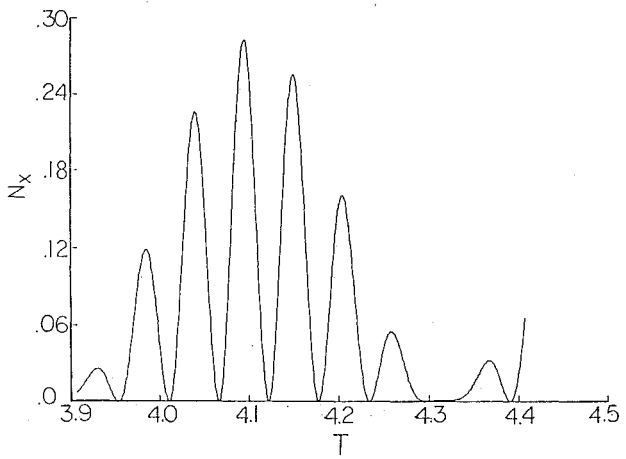

d) Time history of dry friction force, $F_0 = 0.1$ kg, $f = 8$ Hz.

Fig. 3 Cantilevered beam with a pinned dry friction support for $N_g = 10$ kg, $\bar{a}_d = 0.6$.

Referring to the previous treatment, an equivalent viscous damping ratio can be derived as

$$\zeta_n = \frac{1}{\pi M_n \omega_n^2}(D_{12} \text{ or } D_2) \tag{19}$$

Equation (19) can be extended to the more general case of many supports. If there are K span dry friction supports and slip at all supports occurs, the equivalent viscous damping is expressed as

$$\zeta_n = D_K/\pi M_n \omega_n^2 \tag{20}$$

where

$$D_K = \sum_{k=1}^{K} \mu_k N_{gk} \int_0^{a_{d1}} (\phi_n')^2 \, dx + \sum_{k=2}^{K} \mu_k N_{gk} \int_{a_{d1}}^{a_{d2}} (\phi_n')^2 \, dx + \ldots \quad \ldots + \mu_K N_{gk} \int_{a_{d(K-1)}}^{a_{dK}} (\phi_n')^2 \, dx$$

and N_{gk} and μ_k are the normal load and dry friction coefficient at the kth support.

Examples

Here we consider several examples. The first few examples are for a cantilevered beam with different end boundary conditions and a single dry friction support and lead to comparisons with experimental and numerical results. The next few examples consider beams supported at both ends with and without horizontal constraint at one boundary. The last example considers multiple dry friction supports.

Cantilevered Beams

First, we discuss a clamped-free beam with a pinned dry friction support. The equivalent damping ratio can be obtained from Eq. (19) when we set $a_{d1} = a_{d2} = a_d$,

$$\zeta_n = \frac{\mu N g}{\pi M_n \omega_n^2} \int_0^{a_d} (\phi_n')^2 \, dx \tag{21}$$

Figure 2a shows the results for the damping ratio vs $\bar{a}_d$. The maximum values occur when $\bar{a}_d = 1$. In the region of $\bar{a}_d = 0.8 - 1$, the first mode damping is larger than the others. In the region of small $\bar{a}_d$, the second and third modal damping ratios are larger than the first one and the third is larger than the second.

Figure 2b shows natural frequencies vs $\bar{a}_d$ and Fig. 2c the mode shapes for $\bar{a}_d = 0.6$.

Figure 3a compares the responses over a range of excitation frequencies as obtained from the approximate solution and from numerical integration for $\bar{a}_d = 0.6$, $N_g = 10$ kg. The agreement is excellent for large excitation forces, but not so good for small forces, as shown in Fig. 3b. The reason can be explained with the help of Figs. 3c and 3d, which show the time histories of N_x. In this case, small beam deflections occur in the region away from the resonance frequency and stick or slip/stick phenomena appear.

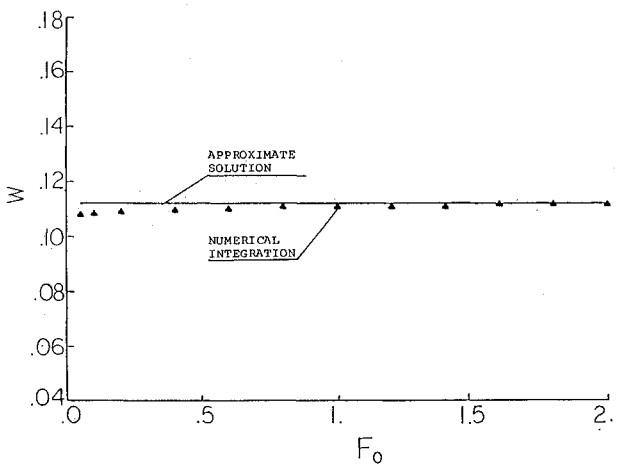

a) Beam deflection vs excitation force.

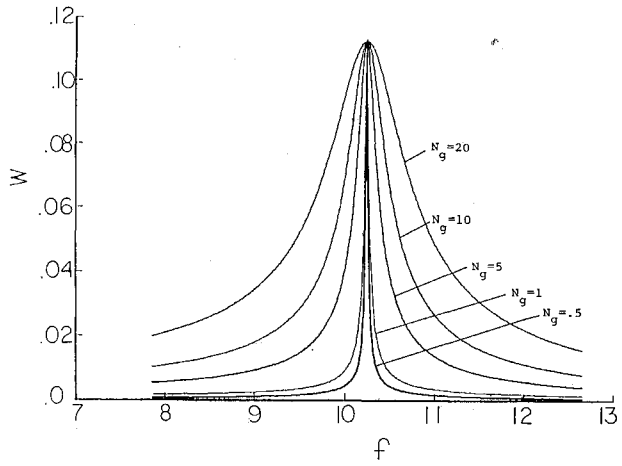

b) Frequency response curve for several normal loads.

Fig. 4 Cantilevered beam with a pinned dry friction support for $N_g/F_0 = 10$.

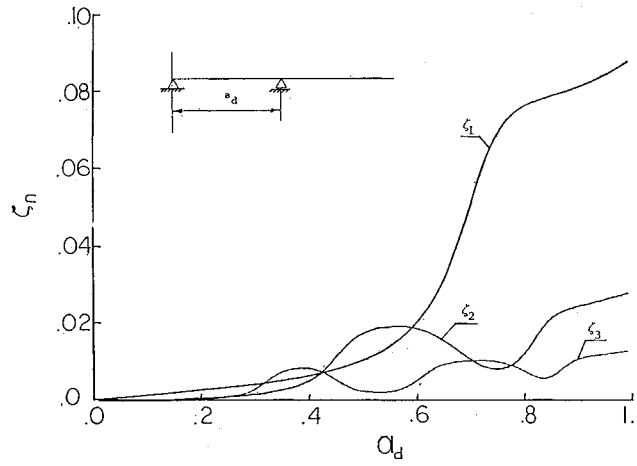

Fig. 5 Modal damping vs $\bar{a}_d$ for supported-free beam with a pinned dry friction support.

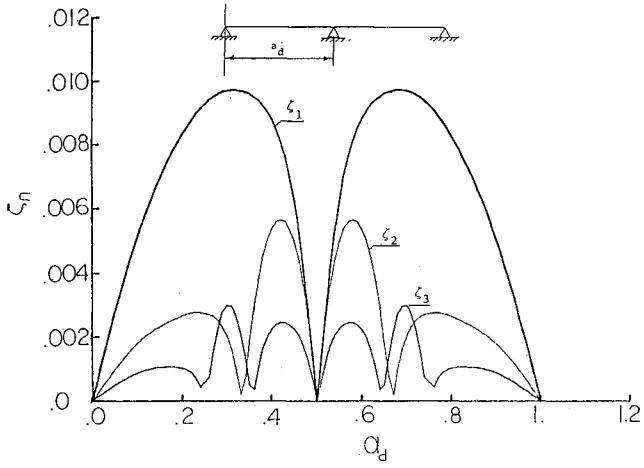

Fig. 7 Modal damping vs $\bar{a}_d$ for pinned supported beam with a pinned dry friction support.

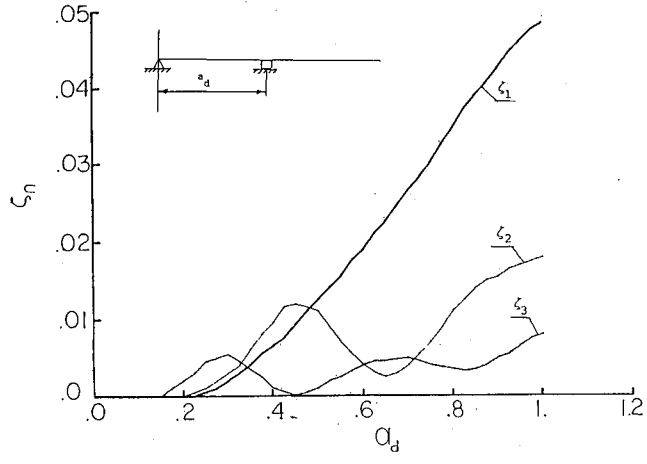

Fig. 6 Modal damping vs $\bar{a}_d$ for supported-free beam with a clamped dry friction support.

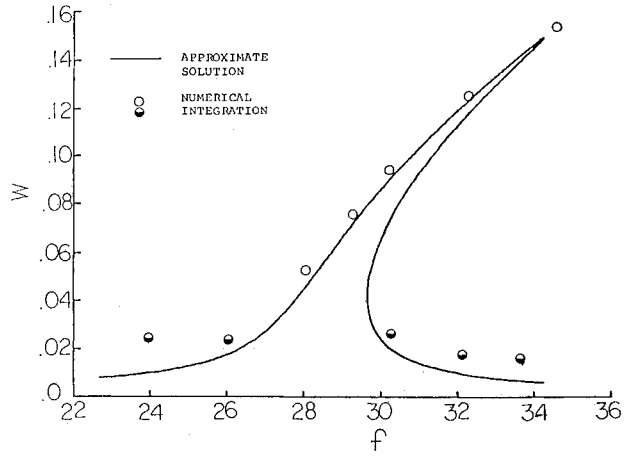

Fig. 8 Frequency response curves for supported beam with a pinned dry friction support and $u(x = 0) = u(x = a) = 0$, $\bar{a}_d = 0.4$.

Figure 4a shows the beam deflection at resonance vs the excitation force for constant ratio $N_g/F_0 = 10$. The comparison of the approximate solution with the numerical integration solution is also shown in the same figure. It is found that the response amplitude is almost independent of excitation force; the agreement between the two results is good. Figure 4b shows frequency response curves for several normal loads in the case of constant normal/excitation force ratio $N_g/F_0 = 10$. The resonance bandwidth enlarges as the normal load increases. However, the amplitude at the resonance frequency has a nearly constant value. This means that increase of the normal load changes only the damping ratio of this system, but does not

change its maximum amplitude.

The second example considered is a pinned supported-free beam with a pinned dry friction support. In this case, although we still use Eq. (21) to calculate the damping, the system modal parameters must be recalculated. Figure 5 shows the results for damping vs $\bar{a}_d$. The shape of these curves is similar to those of Fig. 4a, but the damping ratio is larger than that of Fig. 4a.

The next example is a pinned supported-free beam with a clamped dry friction support. In this case, both a displacement and rotation constraint condition must be simultaneously satisfied. Figure 6 shows the results for damping vs $\bar{a}_d$. It is found that the damping decreases because of the clamped support. The maximum modal damping value is less than about 50%, as compared with that of Fig. 5.

Beam with Both Ends Supported

$u(x = 0) = u(x = a) = 0$

The motion equation can be obtained by substituting $a_{d1} = a_{d2} = a_d$ into Eq. (13). The equivalent damping ratio can be represented as

$$\zeta_n = \frac{\mu N g}{\pi M_n \omega_n^2}\left[\frac{a - a_d}{a}\int_0^{a_d}(\phi_n')^2\,dx - \frac{a_d}{a}\int_{a_d}^{a}(\phi_n')^2\,dx\right] \quad (22)$$

Note that $\zeta_n \to 0$ when $\bar{a}_d \to 0$, 0.5, and 1.0, as expected.

Figure 7 shows the results for damping vs $\bar{a}_d$ for the pinned supported-beam with a pinned dry friction support. The curves are symmetrical about the middle span. The position corresponding to maximum damping is $\bar{a}_d = 0.3$ for the first and third modes and 0.4 for the second mode. In these curves there are several minima.

Figure 8 shows the comparison of the approximate solution and that obtained from the numerical integration for the frequency response curve of the first mode. There is an unstable boundary in the region of 29–34 Hz. It is difficult to determine this boundary line from numerical integration. The good agreement in the stable region indicates that the approximate equivalent damping ratio calculation is reliable.

Figure 9 shows the results of damping vs $\bar{a}_d$ for the supported beam with a clamped dry friction support. The curves again have symmetry about the middle span. As compared with Fig. 7, the maximum damping is smaller by about 8–10% for the first three modes. These are located at $\bar{a}_d = 0.35$ for the first mode, 0.46 for the second mode, and 0.41 for the third mode.

Figure 10 shows the results of damping vs $\bar{a}_d$ for the clamped-supported beam with a pinned dry friction support. As compared with Fig. 7, the maximum damping is little changed. These are located at $\bar{a}_d = 0.27$ for the first mode, 0.61 for the second mode, and 0.72 for the third mode.

$u(x = 0) = 0$, $u(x = a) \neq 0$

The motion equation and equivalent damping ratio will be obtained from Eq. (19), setting $a_{d1} = a_{d2} = a_d$. The damping formula is the same as Eq. (21) with the appropriate modal parameters. Figure 11 shows the results of damping vs $\bar{a}_d$ for the supported beam with a pinned dry friction support. As compared with Fig. 7, it has a very different character. The maximum damping is 6 times higher than that of Fig. 7 for the first mode, 3.6 times for the second mode, and 3.3 times for the

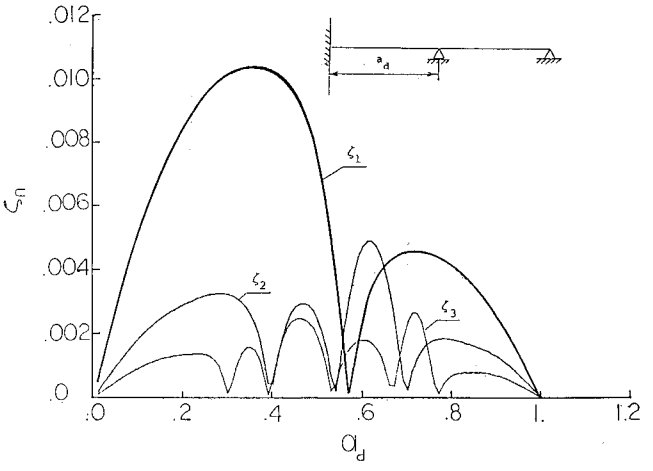

Fig. 10 Modal damping vs $\bar{a}_d$ for clamped-supported beam with a pinned dry friction support.

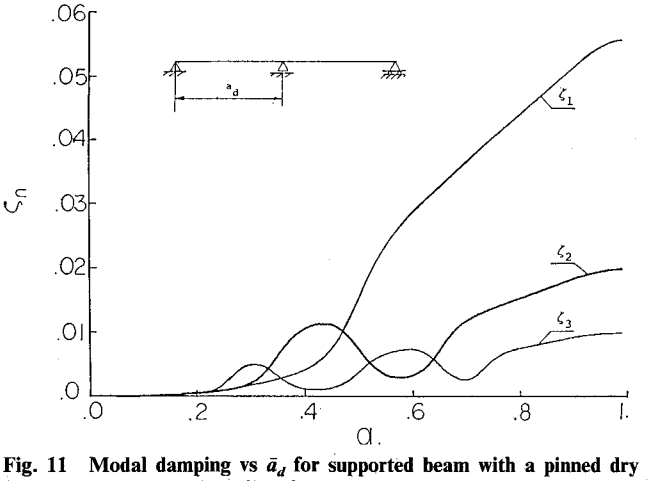

Fig. 11 Modal damping vs $\bar{a}_d$ for supported beam with a pinned dry friction support and $u(x = 0) = 0$, $u(x = a) \neq 0$.

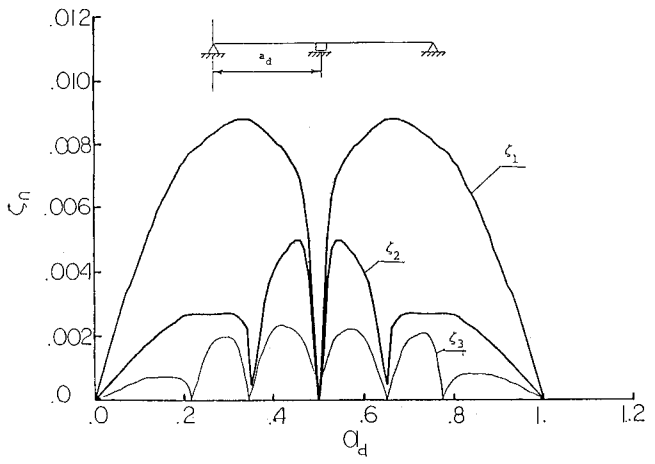

Fig. 9 Modal damping vs $\bar{a}_d$ for supported beam with a clamped dry friction support.

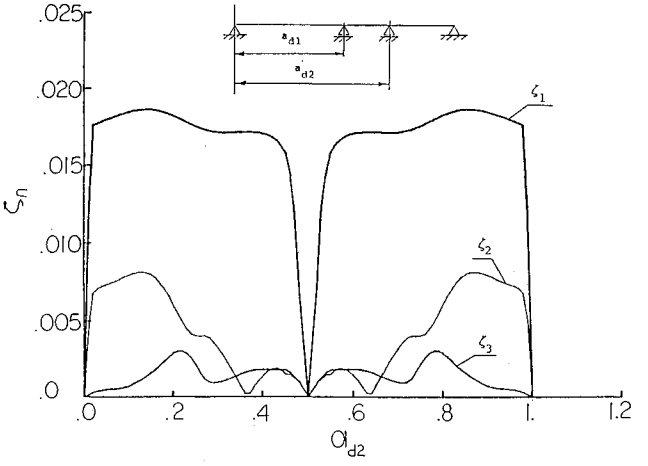

Fig. 12 Modal damping vs $\bar{a}_{d2}$, $\bar{a}_{d1} = 0.5$ for supported beam with two pinned dry friction supports and $u(x = 0) = (x = a) = 0$.

third mode and is located at $\bar{a}_d = 1$. As compared with Fig. 5, the damping ratio is smaller by about 40% for the first mode at $\bar{a}_d = 1$, because of the effect of the boundary pinned support on the natural frequency and mode.

Supported Beam with Multiple Pinned Dry Friction Supports

Supported Beam with Two Pinned Dry Friction Supports

Here, we set $\bar{a}_{d1} = 0.5$ and vary $\bar{a}_{d2}$ from 0 to 1. Figure 12 shows the results of damping for the case of $u(x = 0) = u(x = a) = 0$. These form a symmetrical curve about the middle span. When $\bar{a}_{d2} \to 0$ and 1, the curves abruptly change. When the support position approaches the boundary, the mode shape undergoes a sudden change because the boundary support is transformed from two very close pinned supports to a single pinned support. The maximum damping is located at $\bar{a}_{d2} = 0.82$ for the first mode, 0.84 for the second mode, and 0.78 for the third mode. For the first mode, the damping curve is quite flat. The maximum damping ratio is almost two times higher than that of Fig. 7.

Figure 13 shows the results of damping vs $\bar{a}_{d2}$ for the case of $u(x = 0) = 0$, $u(x = a) \neq 0$. The maximum damping ratio is located at $\bar{a}_{d2} = 1$ for the first mode and 0.43 for the second. The damping curve of the third mode is rather flat. As compared with Fig. 11, it is found that the modal damping decreases as the number of dry friction supports increases. This is because the modal damping varies inversely as the square of the natural frequency. In vibration analysis, it is often convenient to express a real damping in terms of the product of natural frequency and modal damping. The real damping vs the number of dry friction support will be discussed below.

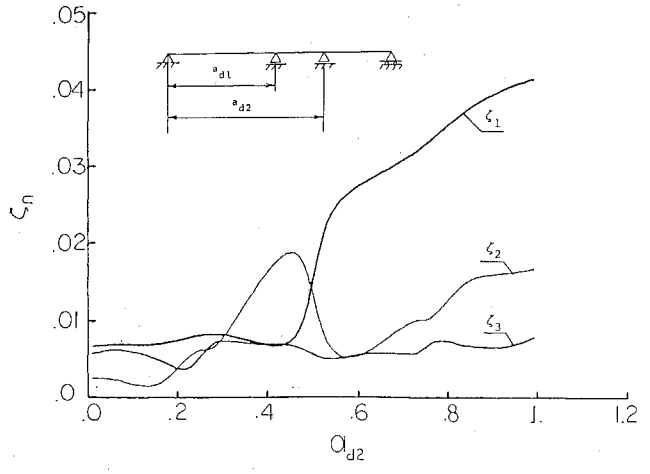

Fig. 13 Modal damping vs $\bar{a}_{d2}$, $\bar{a}_{d1} = 0.5$ for supported beam with two pinned dry friction supports and $u(x = 0) = 0$, $u(x = a) \neq 0$.

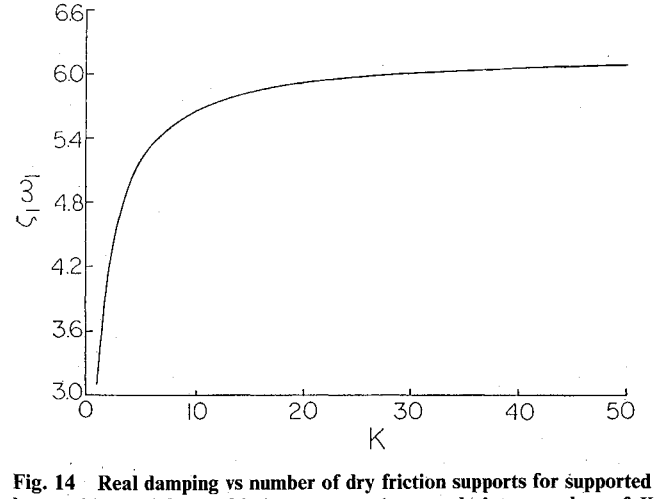

Fig. 14 Real damping vs number of dry friction supports for supported beam with multiple dry friction supports (note: only integer values of K are meaningful).

Supported Beam with Multiple Pinned Dry Friction Supports

As a special example, we assume that K pinned dry friction supports are uniformly distributed along the span and they have the same slipping condition at each support. Figure 14 shows the results of real damping vs the number K of dry friction supports for the case of $u(x = 0) = 0$, $u(x = a) \neq 0$. It is found that the real damping increases as the number K increases and approaches an asymptotic value for large K. On the other hand, the critical damping ratio decreases as K increases.

Effect of Support Reaction on Response

As was stated above, the normal load was assumed constant, i.e., independent of external force. Now, we consider the effect of the change in the normal load due to support reaction. The theoretical model analyzed is shown in Fig. 15a. The analytical method and symbols and subscripts are defined as before.

When slip occurs

$$N_x = \mu(Ng + \Delta N)\ \mathrm{Sign}(a_n \dot{a}_n)$$

where ΔN is the additional normal force support reaction due to the lateral motion of the beam.

Taking a free body diagram about the dry friction support, as shown in Fig. 15b, it follows that

$$\Delta N = S^+ - S^- = -F_0 \sin\omega t + \bar{M}\ddot{a}_n + \bar{K}a_n$$

where

$$\bar{M} = m\left(\int_{a_d}^{a} \phi_n \mathrm{d}x - \int_{0}^{a_d} \phi_n \mathrm{d}x\right), \qquad \bar{K} = EI \left.\frac{\partial^3 \phi_n}{\partial x^3}\right|_{x=0}$$

Using the above results, we undertake a numerical integration. Define δ by the equation

$$\delta = 1 - w_r/w$$

where w_r is the response deflection with the normal force support reaction included.

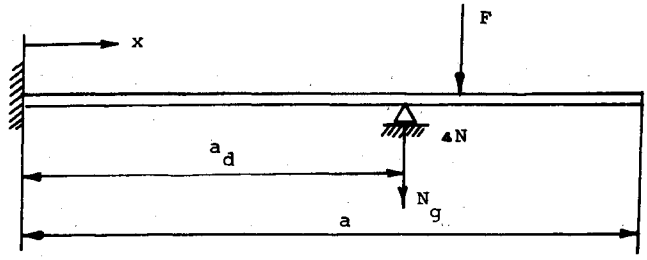

a) Beam geometry.

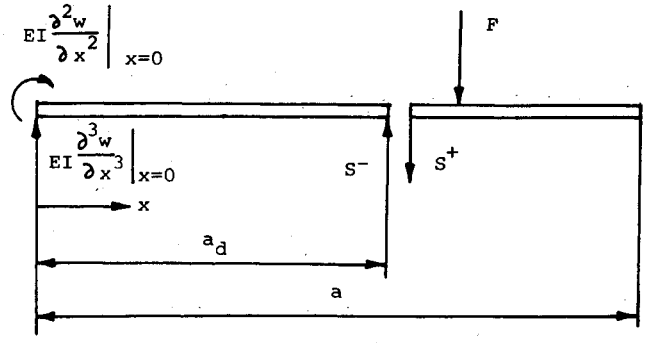

b) Free body diagram about the dry friction support.

Fig. 15 Support reaction.

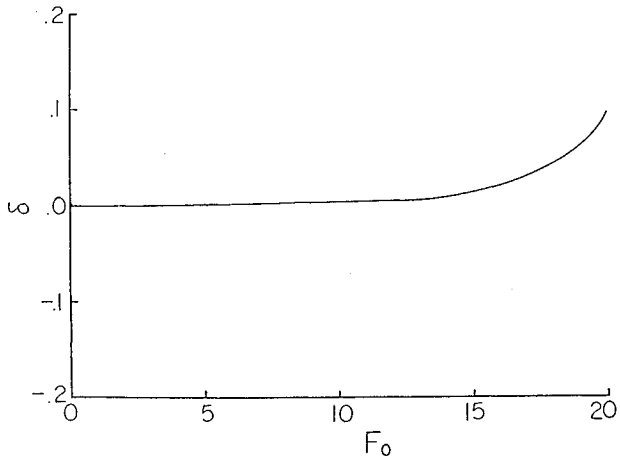

a) δ vs F_0.

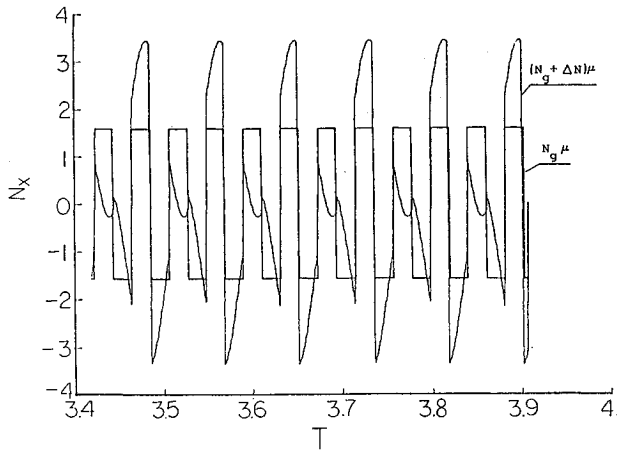

b) Time histories of dry friction force, $F_0 = 10$ kg.

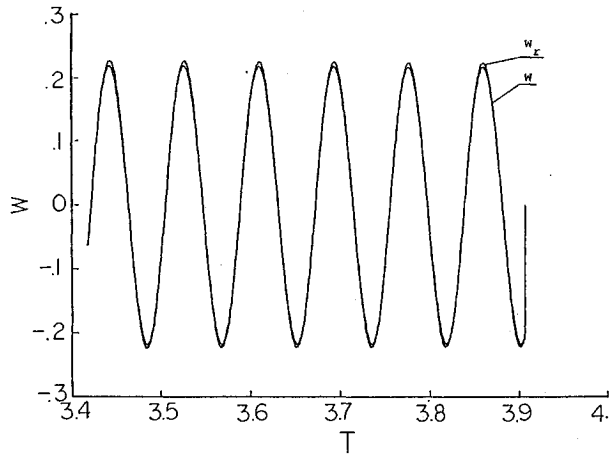

c) Time histories of response deflection, $F_0 = 10$ kg.

Fig. 16 Effect of support reaction on response, $\tilde{a}_d = 0.6$, $f = f_1$, $N_g = 10$ kg.

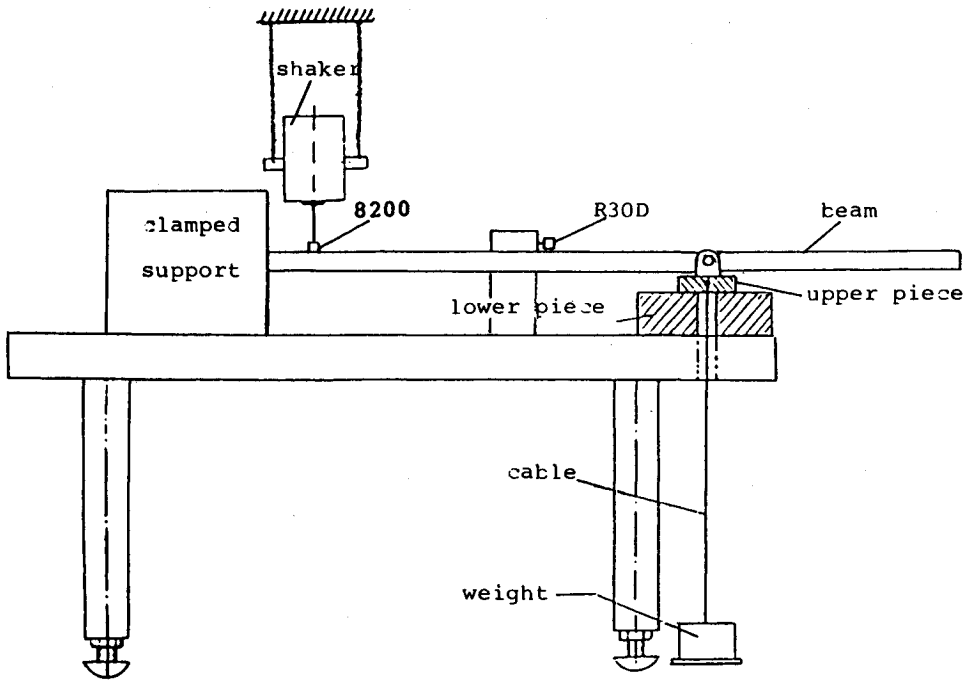

Fig. 17 Experimental setup.

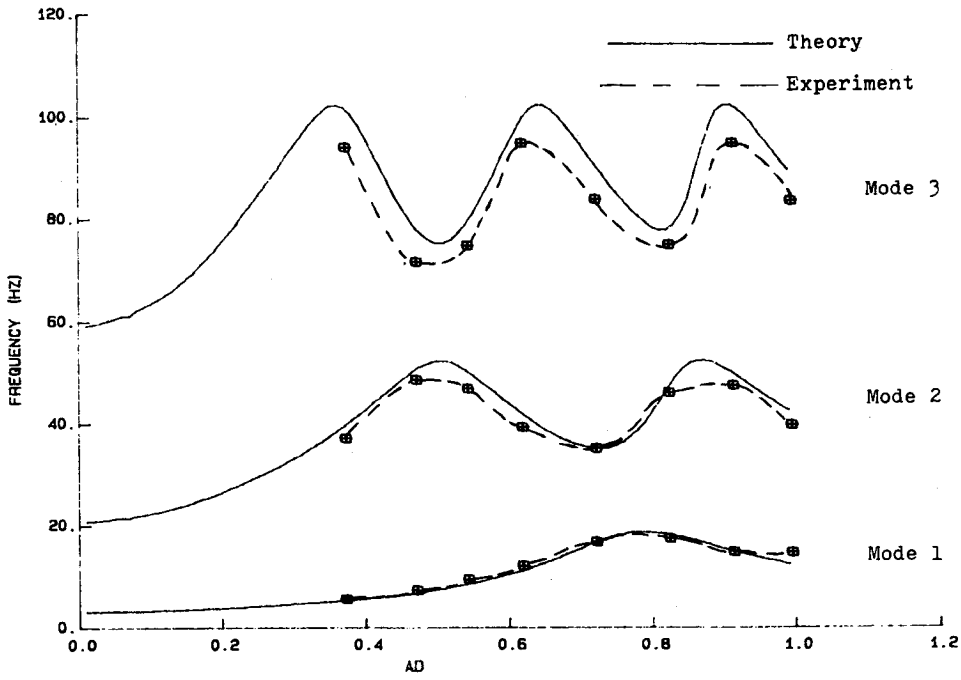

Fig. 18 Cantilevered beam with a pinned dry friction support: natural frequencies vs $\bar{a}_d$.

Figure 16a shows the results of δ vs F_0 for $\bar{a}_d = 0.6$ and the excitation frequency equal to the first natural frequency. When the excitation force is equal to twice the nominal normal load, the response variation only reaches about 10%. This result can be explained by Fig. 16b, which shows typical time histories for the dry friction force. It is found that, in every cycle, the work done by dry friction is very nearly the same with or without the normal force support reaction included. Typical displacement time histories are shown in Fig. 16c.

Experiment

In order to check the validity of the theoretical results, vibration tests were performed on a steel beam, 66.5 cm in length and 2.54 × 0.158 cm in cross section. One end is clamped on a very heavy steel table. The other end is free. A pinned support provides a dry friction element that can be moved to various positions. It has a very light upper test piece made of aluminum. The lower test piece is made of steel and has a polished rubbing surface that is clamped on the same table. A dry friction force is generated by the relative motion between the two test pieces, which are held together with a nominally constant normal load. The normal load is provided by a mass block hung from the center of the upper test piece by a long cable. The experimental setup is shown in Fig. 17.

There are four major components of the vibration test: excitation, measurement, recording, and analysis. An electric magnetic shaker was used to excite the beam. It was driven by a sine generator. In order to reduce the effect of the additional mass of the joint components between the shaker and the beam on the beam vibration characteristics, the position of the driving point is located near the completely clamped end.

The force transducer (B&K 8200) and displacement transducer (R30D) are used to measure the exciting force and displacement response of the beam. The displacement transducer also has only a small added mass. The charge amplifier (B&K 2635) is a portable conditioning amplifier that provides high-voltage output sensitivity for the force. Digital voltage meters were used to record all signals and to analyze natural frequencies and modal damping ratios.

In addition to the effect of added mass, another consideration in the design of the experiment was how to minimize the additional constraint due to joining the R30D with the beam. The contact between the needle and the beam must provide sufficient flexibility to avoid an additional stiffness constraint when large-amplitude vibration occurs. A flexible needle with a pinned end was used to satisfy this requirement.

The coefficient of dry friction used in the response calculation was determined from the value measured in Ref. 2.

Frequency, displacement, and exciting force were continuously recorded by an HP reel-to-reel tape deck. These data were transferred onto a Zonic computer, which averaged a minimum of 20 readings for the 3 modes at each tested point on the beam. The damper was placed at eight different locations on the beam.

Graphs of displacement divided by exciting force vs frequency were then drawn by the computer. From these graphs, the modal damping ratio for the first three modes was calculated by the half-power method.

Measurement of Material Damping

Damping inherent in the beam material was also measured. While it is generally small compared to the damping due to dry friction, it is not negligible.

Material damping values were obtained by removing the shaker and exciting the beam with a modally tuned hammer. The hammer defined the exciting force as the accelerometer measured the displacement. These values were read directly by the computer, which took six averages and produced similar graphs of displacement divided by exciting force vs frequency. Once again, the damping was calculated by the half-power method. A viscous damper was used to model material damping in the theory.

Results

Theoretical results were generated for the following parameters: natural frequency, modal damping (with and without material damping), and mode shapes. Experimental results were obtained for the dry friction damper placed in turn at eight points along the beam, from $\bar{a}_d = 0.372$ (near the clamped end of the beam) to $\bar{a}_d = 0.944$ (near the other end of the beam). A 5 kg normal force was used.

The measured natural frequency results (Fig. 18) were very close to the calculated frequencies. Agreement is particularly good for the first two modes, while the third mode frequencies are systematically slightly lower than calculated, but still follow

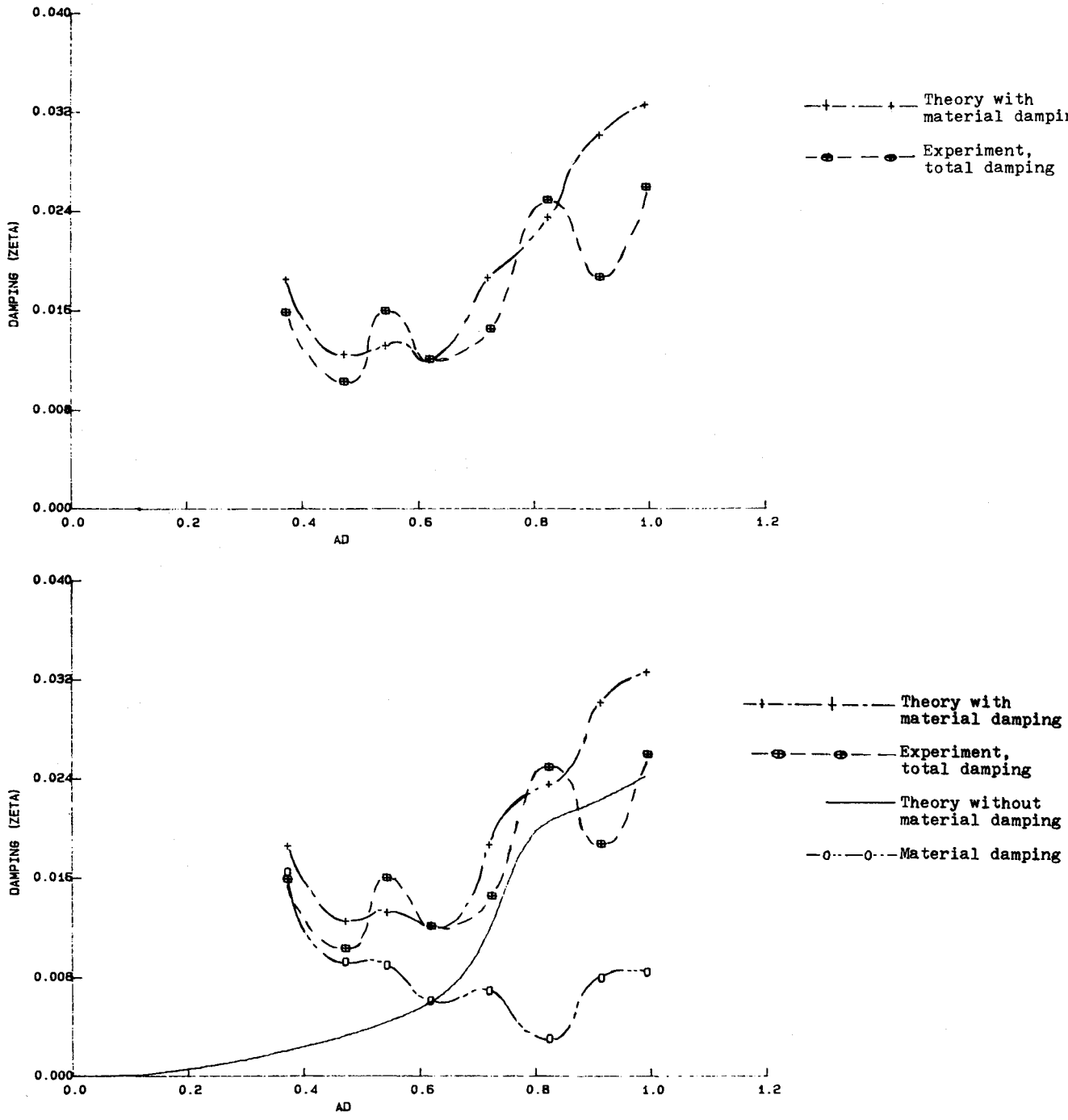

Fig. 19 Cantilevered beam with a pinned dry friction support: modal damping vs $\bar{a}_d$, mode 1.

the trend predicted by the theory.

Damping results for the first mode can be seen in Fig. 19a where the experimental results are compared to the theoretical values (which include the measured material damping). A more detailed comparison is given in Fig. 19b. This graph shows the theory without material damping, material damping only, theory with material damping, and experimental results for total damping. Note here that the material damping generally decreases as $\bar{a}_d$ becomes larger, until the end of the beam is approached where it increases again.

The smallest $\bar{a}_d$ shows a measured material damping actually larger than that measured for total damping. This is probably the result of difference in the experimental procedure used to determine material damping vs total damping, as well as the effect the shaker may have had upon the total damping measurement. The shaker was removed for the material damping experiment. In Fig. 19a, note how closely the experimental values follow the theory with the exception of $\bar{a}_d = 0.914$. Damping tends to increase for the larger $\bar{a}_d$.

Similar results are shown for the second mode in Fig. 20. Note that in Fig. 20a the experimental values also follow the trend of the theory very well. The largest discrepancy occurs at the end of the beam. Again, the larger $\bar{a}_d$ values provide more damping.

The final (third) mode that was analyzed shows the largest differences among all the results. See Fig. 21. The experimental trends are similar to those of the theory. However, the theory is consistently lower than the experiment for the third mode (Fig. 21a). Nevertheless, the critical damping ratio predicted by theory varies from experiment by only 0.008 at most.

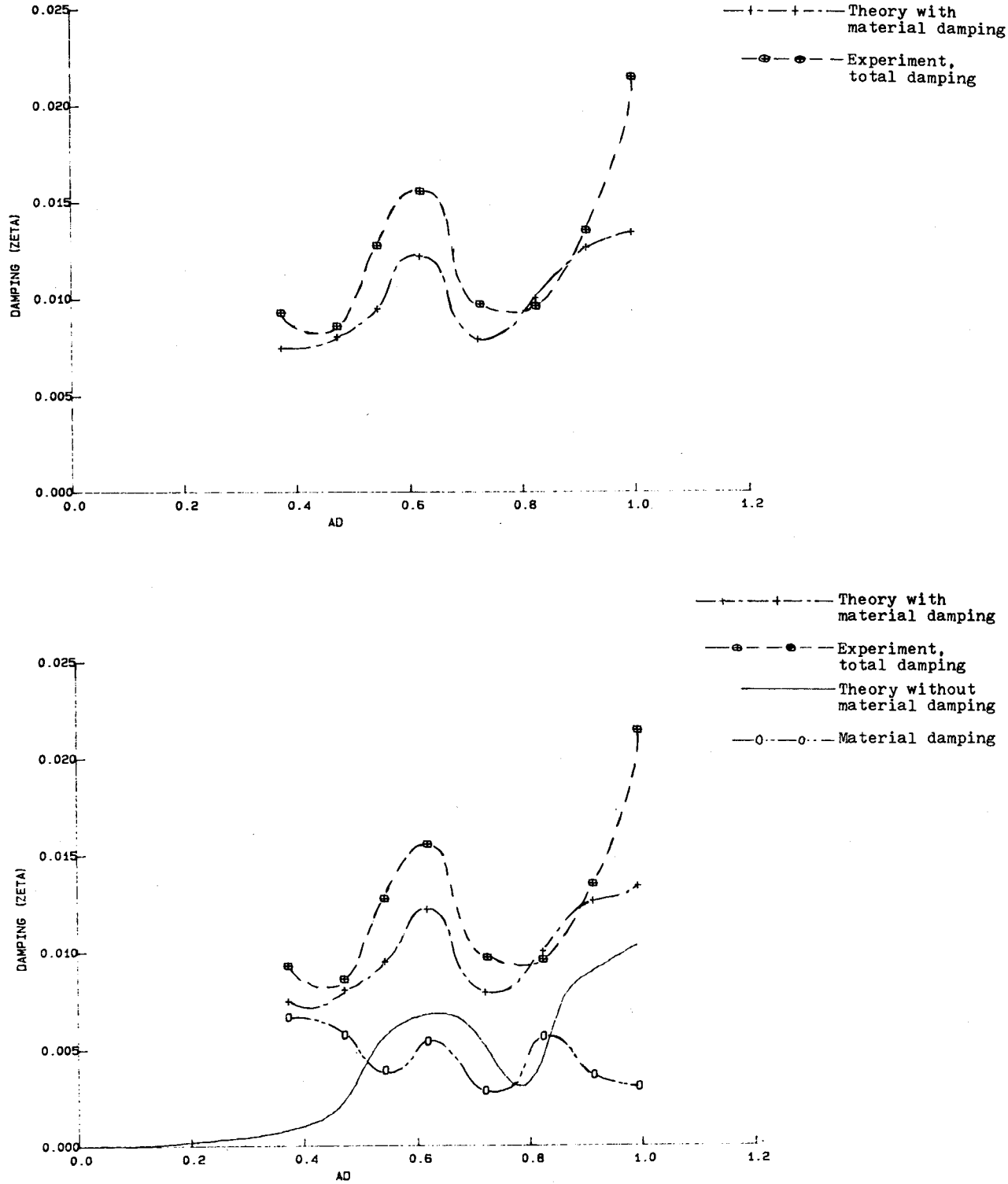

Fig. 20 Cantilevered beam with a pinned dry friction support: modal damping vs $\bar{a}_d$, mode 2.

Conclusions

1) The numerical simulation results have shown that the equivalent linear viscous damping approximate solution has good accuracy for the case where the lateral motion is sufficiently large that slip occurs.

2) The equivalent damping ratio is dependent upon the position of the dry friction support.

3) In general, the modal damping ratio is also dependent on the end boundary conditions. From the point of view of increasing modal damping, the free end is better than pinned and the pinned end is better than clamped. For the pinned-pinned beam, the boundary support without horizontal constraint is better than that with one.

4) Generally, the pinned dry friction support can provide more modal damping than that of the clamped.

5) Multiple span dry friction supports are not expected to provide more modal damping than a single dry friction support, but they can provide more real damping.

6) The effect of support reaction at a dry friction support on response (modal damping ratio) is very weak.

7) Theory provides an excellent prediction for the natural frequency for a beam with a dry friction vibration damper

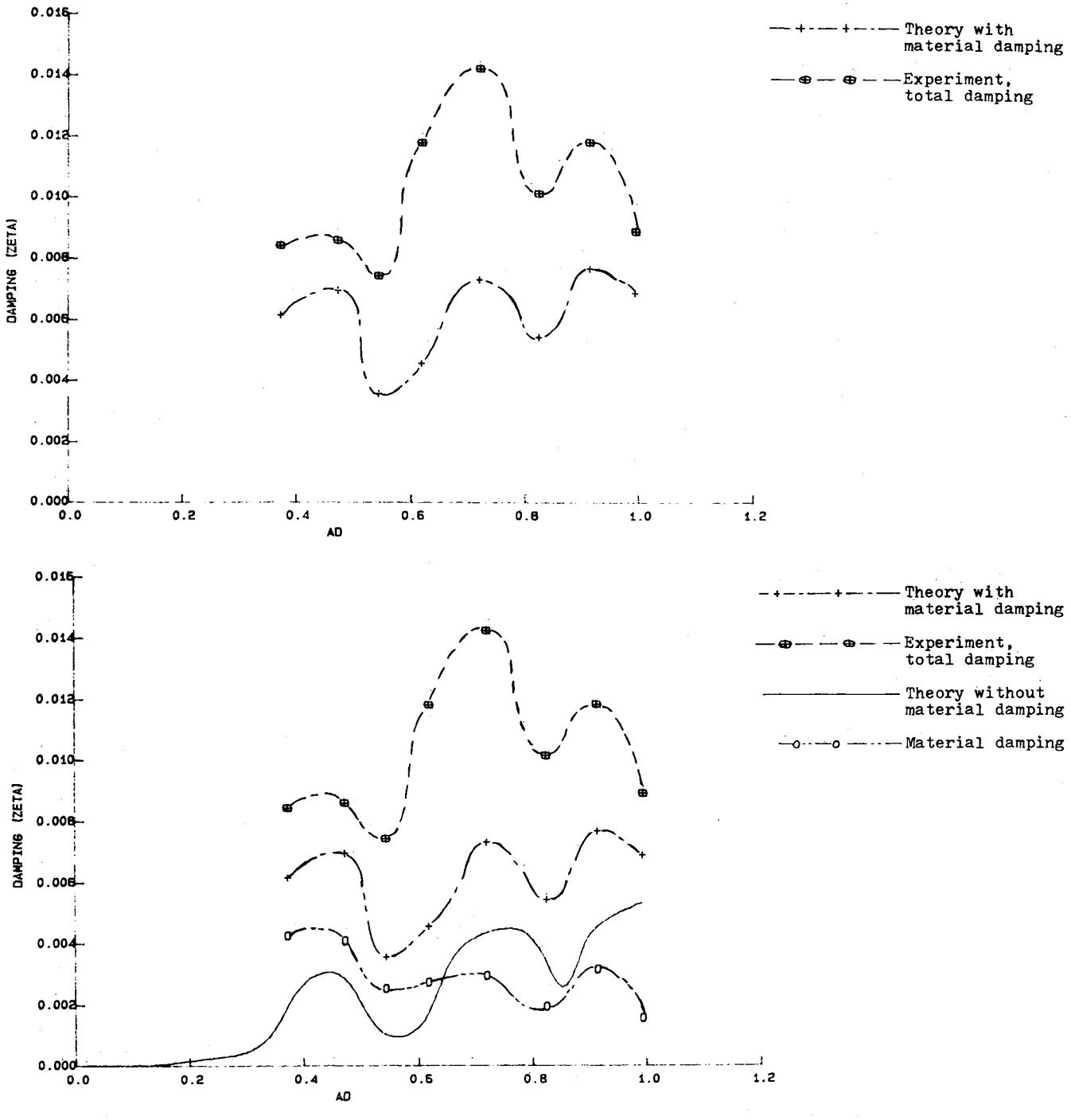

Fig. 21 Cantilevered beam with a pinned dry friction support: modal damping vs $\bar{a}_d$, mode 3.

located at any position.

8) Good agreement for damping between theory and experiment is generally achieved when material damping is included in the theory.

Acknowledgment

This work was supported by the U.S. Air Force Office of Scientific Research, Grant 83-0346. Dr. Anthony Amos was the technical monitor.

References

[1]Dowell, Earl H., "Damping in Beams and Plates Due to Slipping at the Support Boundaries, Part 1: Theory," *Journal of Sound and Vibration*, Vol. 105, No. 2, 1986, pp. 243–253.

[2]Tang, D. M. and Dowell, E. H., "Damping in Beams and Plate Due to Slipping at the Support Boundaries, Part 2: Numerical and Experimental Study," *Journal of Sound and Vibration*, Vol. 108, No. 3, 1986, pp. 509–522.

[3]Den Hartog, J. P., *Mechanical Vibrations*, McGraw-Hill, New York, London, 1934.

[4]Timoshenko, S., Young, D. H., and Weaver, W. Jr., *Vibration Problems in Engineering*, Wiley, New York, 1974.

[5]Dowell, E. H. and Schwartz, H. B., "Forced Response of a Cantilever Beam with a Dry Friction Damper Attached, Part I: Theory, Part II: Experiment," *Journal of Sound and Vibration*, Vol. 91, No. 2, 1983, pp. 269–291.

[6]Jones, D. I. G., "Vibrations of a Compressor Blade with Slip at the Root," U.S. Air Force Wright Aeronautical Laboratories, Rept. AFWAL-TR-80-4003, April 1980.

[7]Beards, C. F., "The Damping of Structural Vibration by Controlled Interfacial Slip in Joints," *Transactions of ASME, Journal of Vibration, Acoustics, Stress, and Reliability in Design*, Vol. 105, July 1983, pp. 369–373.

[8]Zmitrowicz, A., "A Vibration Analysis of a Turbine Blade System Damped by Dry Friction Forces," *International Journal of Mechanical Sciences*, Vol. 23, No. 12, 1981, pp. 741–761.

[9]Jezequel, L., "Structural Damping by Slip in Joints," *Transactions of ASME, Journal of Vibration, Acoustics, Stress, and Reliability in Design*, Vol. 105, Oct. 1983, pp. 497–504.

[10]Plunkett, R., "Friction Damping," *Damping Applications for Vibration Control AMD*, Vol. 38, ASME, New York, 1980.

[11]Pratt, T. K. and Williams, R., "Nonlinear Analysis of Stick/Slip Motion," *Journal of Sound and Vibration*, Vol. 74, No. 4, 1981, pp. 531–542.

[12]Dowell, E. H., "Component Mode Analysis of Nonlinear and Nonconservative Systems," *Journal of Applied Mechanics*, Vol. 47, March 1980, pp. 172–176.

[13]Dowell, E. H., "Free Vibrations of a Linear Structure with Arbitrary Support Conditions," *Journal of Applied Mechanics*, Vol. 38, Sept. 1971, pp. 595–600.